Interaction of Nitric Oxide with Molecular Adlayers Adsorbed on Rh(111)

Vittorio Fiorin,* Martin R. S. McCoustra, and Michael A. Chesters

School of Chemistry, University of Nottingham, University Park, Nottingham NG7 2RD, U.K.

Received: December 5, 2003; In Final Form: March 15, 2004

The interaction of nitric oxide (NO) with well-ordered carbon monoxide (CO) and ethylidyne (CCH_3) overlayers chemisorbed on Rh(111) has been studied. State-resolved rotational and translational energy distributions of NO scattered from the CO and CCH_3 adlayers on Rh(111) at 300 K were measured using (1+1) resonance-enhanced multiphoton ionization. To compliment these studies, the adsorption of NO onto the same surfaces at 120 K was investigated, using a combination of reflection−absorption infrared spectroscopy, temperature-programmed desorption, and collision-induced desorption. Rotational state and velocity distributions indicate that the NO dynamics show a dominance of scattering via trapping desorption over direct inelastic processes, even at the relatively high incident translational energy (47 kJ mol^{-1}) and the surface temperature (300 K) used. This is in stark contrast with the scattering dynamics of the same molecule from the same adlayers adsorbed on Pt(111). The study of the static interaction of NO with the same adlayers at 120 K revealed that adsorption of NO takes place in an unusual second adlayer on top of both CO and CCH_3 overlayers. In particular, it was found that the NO molecule adsorbs with its internuclear axis parallel to the surface. The potential well depth of this particular gas−surface system has been estimated from desorption experiments to be 36 kJ mol^{-1} for both adlayers. However, the CO adlayer showed a greater propensity for the accommodation of the NO molecule in comparison with the CCH_3 adlayer. This is also consistent with the conclusions from the dynamical studies.

Introduction

The study of the scattering dynamics of small molecules from well-ordered surfaces has received a great deal of attention since state-selective experimental methods have allowed detailed measurements of the energy disposal following such molecule−surface encounters.[1] While the velocity distribution of scattered molecules can be investigated using standard time-of-flight (TOF) methods,[2] it has been the combination of molecular beams with laser-based spectroscopies that has revolutionized the investigation of the internal state population distributions of scattered molecules.[3] This powerful combination has, at least in part, allowed the determination of the energy balance in gas−surface scattering events.

Since the very first gas−solid scattering experiments utilizing noble gases, e.g., xenon, and flat surfaces, e.g., Pt(111), there has been the obvious necessity of distinguishing and characterizing different scattering channels, i.e., direct inelastic scattering and trapping desorption scattering.[4] Experiments measuring TOF and angular distributions of scattered particles, either atoms or molecules, from clean surfaces opened up the possibility of understanding those different mechanisms which are governed not only, though principally, by the thermodynamics of the system, but also by the characteristic potential energy surface of the system.[5] For incident atoms or molecules whose translational energies are greater than the gas−solid interaction potential well depth, the direct inelastic scattering channel is revealed by a narrow angular distribution peaked toward the specular direction and a translational energy distribution broadened only slightly from that incident on the surface. On decreasing the incident energy, the angular distribution broadens and shifts toward the surface normal. This is also accompanied by a substantial increase in the width of the final translational energy distribution, reflecting a longer gas−surface interaction time in which multiple collisions, and hence accommodation of the atoms or molecules, with the surface are likely. This is illustrated clearly in comparing the scattering of oxygen and argon from Ag(111) at room temperature.[6]

The dynamics of nitric oxide (NO) scattering from clean surfaces such as Ag(111)[7−12] and Pt(111)[13−18] has been extensively studied. In contrast, NO scattering from ordered molecular adlayers adsorbed on single-crystal surfaces has received less attention. The importance of studying the influence of an adsorbate on the dynamics of scattering lies in its direct relevance to catalysis, where molecules may be interacting with a precovered catalyst surface. Early experiments performed by Ertl and co-workers involved scattering of NO from Pt(111) precovered with NO, C, and O, and its comparison to scattering from the clean surface.[19,20] The presence of the adlayer was seen to reduce the sticking probability of the NO and consequently the scattering in the trapping desorption channel seen on the clean surface. Increasing the NO incident translational energy and surface temperature resulted in a peaking of the angular distribution of the scattered NO in the specular direction. This is consistent with direct inelastic scattering from the adsorbate-precovered surface compared with the clean surface. NO rotational state distribution measurements were consistent with these observations in showing poor accommodation with the surface. It is clear that the presence of the adlayer significantly modified the interaction between the NO and the surface. Another elegant example on how an adlayer can dramatically change the scattering dynamics is to be found in the scattering of NO from the clean and atomic hydrogen

* To whom correspondence should be addressed. Present address: Department of Chemistry, University of Cambridge, Lensfield Road, Cambridge CB2 1EW, United Kingdom. E-mail: vf208@cam.ac.uk.

10.1021/jp031290j CCC: $27.50
Published on Web 06/24/2004

covered Ru(0001) surfaces.[21] The angular distribution of NO scattering from clean Ru(0001) is very broad for an incident NO translational energy of 160 kJ mol^{-1}. If atomic hydrogen is preadsorbed on the surface, then the NO angular distribution appears as a very narrow cone around the specular direction for the same initial conditions. The chemisorption of hydrogen makes the Ru surface inert with respect to the NO molecule and effectively turns the surface into a molecular mirror.

At the other extreme of adsorbate complexity, NO scattering has been investigated from organized organic monolayers self-assembled on a glass support.[22−24] Rotational distributions, measured for incident translational energies in the range of 14−34 kJ mol^{-1}, indicated that accommodation takes place for collision energies below 30 kJ mol^{-1}. The scattered NO rotational temperature was found to be very close to the surface temperature, especially for low rotational quantum states. In this particular interface, the thermal behavior is not explained in terms of the potential well depth, as the gas−surface interaction is very weak for these systems. Instead, the conclusion was that the accommodation results from the surface scattering, which is thought to be occurring from a soft surface, due to the space available between chains of the adsorbate molecules. This soft collision results in a lengthened interaction (compared with a clean metal surface) in which momentum transfer is very efficient and energy flows back and forth between the NO and the surface.[22]

More recently, Ainsworth et. al.[25,26] have investigated energy disposal as a result of collisions of NO with carbon monoxide (CO) and ethylidyne (CCH_3) layers adsorbed on Pt(111). These systems were roughly of the same mass but with significantly different vibrational properties, so it was hoped this would allow us to investigate the role of adsorbate internal structure on gas−surface scattering processes in more detail. TOF measurements of translational energy distributions and resonance-enhanced multiphoton ionization (REMPI) measurements of rotational energy distributions of scattered NO molecules for incident translational energies in the range of 10−50 kJ mol^{-1} and for surface temperatures from 100 to 300 K were made. Both direct inelastic scattering and trapping desorption were observed. Pure trapping desorption is only revealed at low surface temperatures and low collision energies. On the other hand, direct inelastic scattering is isolated at high surface temperatures and high incident NO translational energy. Furthermore, a considerable degree of translational energy loss, ca. 60%, was observed in the direct scattering channel. Both surfaces exhibited similar behavior with only the trapping desorption component found to be slightly more dominant for NO scattering from the CO adlayer compared with the scattering from the CCH_3 adlayer. This was attributed to the presence of a stronger dipolar interaction between incoming NO and the CO adlayer than with the CCH_3 adlayer.

The present study returns to the interaction of NO with CO and CCH_3 adlayers but on this occasion chemisorbed on Rh(111). Measurements were made at a range of incident NO energies and surface temperatures and compared to those previously reported for the Pt(111) substrate.[25,26] In principle, one might expect similar behavior, given that the adsorbed layers may screen any possible influence of the metal substrate. Remarkably, however, the scattering behavior of the two sets of systems could not be more dissimilar. In contrast to the Pt(111) substrate, scattering from the Rh(111)-bound substrate at 300 K was dominated by trapping desorption with a NO residence time significantly in excess of the time scale of the REMPI technique used for TOF and rotational state distribution measurements. Additional measurements at low surface temperatures combining reflection−absorption infrared spectroscopy (RAIRS), temperature-programmed desorption (TPD), and collision-induced desorption (CID) indicate that adsorption of NO occurs onto the preadsorbed molecular layer, rather than directly onto the metal surface. Such behavior is entirely consistent with an interaction well depth for the NO of 35−40 kJ mol^{-1} (cf. 5−10 kJ mol^{-1} on the Pt(111) substrate[25,26]).

Experimental Section

All experiments were carried out in a stainless steel ultra-high-vacuum (UHV) chamber, which has been described in detail previously.[27,28] Essentially, the UHV chamber is pumped by a 9 in. liquid nitrogen trapped oil diffusion pump (Edwards E09) to a base pressure of better than 1×10^{-10} Torr after baking. The UHV chamber is coupled with a triply differentially pumped supersonic molecular beam system and contains two levels. The upper level includes an argon ion sputter gun (VG Microtech AG21), an electron gun (VG Scientific LEG 22), and a hemispherical electron energy analyzer (VG Microtech Clam 100) for Auger electron spectroscopy (AES). The lower level comprises a fixed quadrupole mass spectrometer (VG Quadrupole Micromass Q7) in the line of sight with the molecular beam entrance, a rotatable quadrupole mass spectrometer (VG Quadrupole Micromass PC300D) used for monitoring residual gas partial pressures and for TPD measurements, two differentially pumped KBr windows for RAIRS experiments, and a microchannel plate detector (Photek VPM218) for ion detection used in REMPI experiments.

RAIR spectra were recorded using a Fourier transform infrared spectrometer (Bio-Rad FTS-60A) with infrared radiation incident on the sample at a grazing angle of approximately 87° with respect to the surface normal. The reflected light was collected and focused on a liquid nitrogen cooled mercury cadmium telluride (MCT) detector. Spectra were recorded at a resolution of 4 cm^{-1} by taking the ratio of 1024 co-added background and sample spectra.

The rotational quantum state distributions of the incident NO molecular beam and those of the NO scattered molecules were determined using the (1+1) REMPI technique through the $\gamma(0,0)$ rovibronic transition (i.e., $A^2\Sigma^+(v=0) \leftarrow X^2\Pi_i(v=0)$) of the molecule. Tunable laser light at around 225 nm was generated using a Nd^{3+}-YAG pumped dye laser system (Spectron Laser Systems SL803 and SL4009) operating at a repetition rate of 10 Hz. The UV light, with a pulse energy of 300 μJ, was then focused in the scattering region of the UHV chamber at approximately 20 mm from the scattering substrate. Ions produced in the REMPI process were collected and amplified by the microchannel plate. This output signal was further amplified (EG&G Ortec 9301) before being recorded by a digital oscilloscope (LeCroy 9420). The supersonic molecular beam was mechanically chopped by a rotating blade, producing a 400 Hz train of pulses of 28 μs duration. The frequency was monitored by an optocoupler sensor which itself acts as a trigger for the laser firing. A frequency divider circuit and a digital delay generator (Stanford Research Systems DG535) ensured the necessary synchronization between the molecular beam and the laser beam. Time-of-flight measurements of the incident molecular beam and the scattered beam are measured by fixing the laser wavelength for a particular rovibronic transition and varying the time delay on a microsecond time scale.

The surface sample consists of an 8 mm diameter rhodium single-crystal disk cut to within 0.5° of the (111) plane. It can be heated resistively to 1300 K and cooled to 100 K through a

liquid nitrogen reservoir. The surface temperature is monitored by a K-type chromel−alumel thermocouple spot-welded onto the edge of the crystal. Initial cleaning of the surface consisted of several cycles of argon ion sputtering and annealing at 1000 K for 2 min. Routine cleaning cycles consisted of oxidation by exposing the surface to an oxygen pressure of 1×10^{-7} Torr for 10 min and a surface temperature of 700 K, and subsequent annealing at 1100 K for 3 min. The cleanness of the surface was checked by means of AES and RAIRS measurements of adsorbed CO. The latter is an effective probe of surface cleanness, since the RAIRS features of CO are known to be crucially sensitive to surface contamination. The surface was considered clean when exposing the Rh(111) crystal to 10 langmuirs of CO (1 langmuir $= 1 \times 10^{-6}$ Torr s) resulted in a CO RAIR spectrum having two bands at characteristic frequencies: one major peak between 2065 and 2068 cm^{-1} corresponding to the C−O stretch of CO adsorbed in an atop site, and a second less pronounced and broader peak around 1860 cm^{-1} corresponding to the C−O stretch of CO adsorbed on a multiply coordinated site of the rhodium surface. This CO adlayer was also used in the scattering experiments. The ethylidyne adlayer was formed by exposing the clean Rh surface to 5 langmuirs of C_2H_4 at room temperature, which is sufficient for the species to dehydrogenate and rearrange to form a saturated adlayer of chemisorbed CCH_3. The ethylidyne RAIR spectrum shows resonances at 1124, 1337, and 2872 cm^{-1} which can be assigned to the ν_s(C−C), $\delta_s(CH_3)$, and ν_s(C−H) vibrations, respectively.[29] Previous measurements indicate that this layer exhibits a p(2×2) structure corresponding to a saturation coverage of 0.25 monolayer (ML).[30]

The Pt(111) single crystal was that used in the previous study by Ainsworth et al.,[25,26] and details of the cleaning and characterization procedures are found therein.

Results and Discussion

I. Scattering Dynamics of NO from CCH_3 and CO Adlayers on Rh(111) at 300 K. NO scattering measurements were made from the 300 K adlayer surfaces for a range of incident translational energies up to ca. 50 kJ mol^{-1} with fixed incident and scattering angles of the NO beam of 20° with respect to the surface normal. The incident translational energy was selected simply by seeding the NO molecule in an admixture with hydrogen, helium, and argon. Mixture compositions were chosen to produce good signal-to-noise ratios with respect to the laser detection system. Nozzle heating was avoided, as this would rotationally excite the transitionally cold NO molecules in the beam. Theoretical values of the incident translational energy deduced assuming ideal expansion of the gas mixture[31] were confirmed experimentally by TOF measurements. In such measurements, the REMPI ion signal is acquired as a function of the time delay at a fixed laser frequency. For the incident beam, this is set to one of the $^2\Pi_{1/2}$ band heads of the $\gamma(0,0)$ transition corresponding to transitions originating from $J'' = 1.5$, 2.5, and 3.5 in the $R_{11} + Q_{21}$ band. The same frequency is used in TOF studies of scattered NO as representative of a population of NO molecules with a low rotational energy. In contrast TOF measurements made on the overlapped $J'' = 20.5$ state of the $R_{11} + Q_{21}$ branch and $J'' = 15.5$ state of the R_{21} branch around 225.7 nm are chosen as representative of rotationally excited NO.

The analysis of the acquired TOF data has been described in detail previously.[25] Here only a brief summary is given. In the case of the incident beam, the measured velocity distribution is the result of a convolution of the finite width of the chopper slit and the velocity distribution, $f(v)$, which depends on the hydrodynamic speed ratio, h, the ratio between the central velocity of the distribution (i.e., the stream velocity) and the spread of the distribution, α. The distribution $f(v)$ can be written as

$$f(v) = A_0 v^3 \exp\left[-\left(\frac{v - v_s}{\alpha}\right)^2\right] \quad (1)$$

where A_0 is a scaling factor, v_s the stream velocity, and α the velocity spread, which is given by

$$\alpha^2 = (2k_B/m)T_{parallel} \quad (2)$$

The hydrodynamic speed ratio, $h = v_s/\alpha$, is used to calculate the mean square velocity, $\langle v^2 \rangle$, as described for a molecular beam with $h \gg 1$ by

$$\langle v^2 \rangle = \alpha^2\left(h^2 - \frac{3}{2h^2 + 3} + 3.5\right) \quad (3)$$

From this, the mean final translational energy can simply be obtained by the relationship

$$\langle E_f \rangle = \frac{1}{2} m \langle v^2 \rangle \quad (4)$$

Values of the final energy deduced in this way can be compared with those predicted assuming ideal free jet expansion in the generation of the molecular beam mixture, namely, using

$$E = \frac{1}{2} m v^2 = \frac{1}{2} m\left[\frac{2\gamma_{av} k_b T_0}{(\gamma_{av} - 1) m_{av}}\right] \quad (5)$$

where m is the mass of the gas of interest, γ_{av} is the weighted average of the ratio between the specific heat, C_p, and C_v of the components in the gas mixture, T_0 is the gas temperature of the source, and m_{av} is the weighted average of the molecular masses of the seed gas and the gas of interest.

Figure 1a shows the fit (solid line) of the experimental TOF data (open circles) of the 7% NO in He (28%) and H_2 (65%) incident molecular beam at room temperature. Table 1 reports the output parameters of the velocity distribution, $f(v)$, and the calculated physical quantities from the parameters. As can be seen, the incident beam TOF agrees well with the theoretical prediction, in terms of both translational energy and central velocity. The parameters characterizing the incident beam are then used in the analysis of the scattered NO beam.

The result of the scattering event can be described assuming that the molecule escapes the surface principally via two distinctive mechanisms, namely, direct inelastic scattering and trapping desorption scattering, occurring either simultaneously or separately. This can be simply formalized in what is called the *response function*, following the approach described by Auerbach.[33] This function is dependent only upon the initial and final velocities of the gas molecule for a given angle of incidence and detection. The response function can be written as

$$R(v_f, v_i) = A_1 {v_f}^3 \exp\left[-\left(\frac{v_f - \gamma v_i}{\alpha_i}\right)\right] + A_2 {v_f}^3 \exp\left[-\left(\frac{v_f}{\alpha_2}\right)^2\right] \quad (6)$$

The first term is used to describe the direct inelastic scattering, the form of which is similar to the expression for the incident molecular beam. It contains three parameters, the direct inelastic intensity factor, A_1, the direct inelastic width, α_1, and the

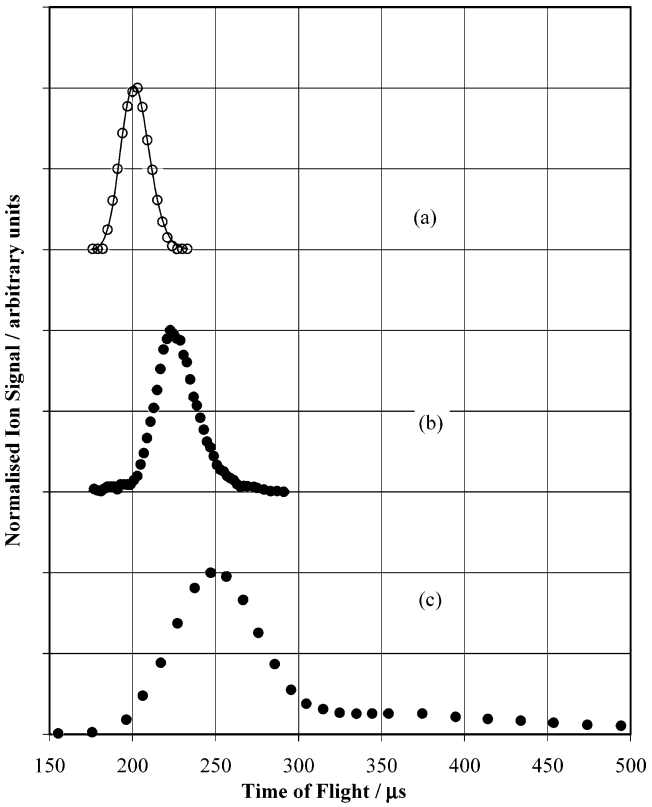

Figure 1. (a) TOF profiles of the 7% NO in He and H_2 incident molecular beam. Open circles are the experimental data, and the solid line is the fitted distribution. The parameters for the fit are given in Table 1. (b) TOF profile for the scattered NO from Rh(111)−CCH_3 at room temperature. (c) TOF profile for the scattered NO from Pt(111)−CCH_3 at room temperature.

TABLE 1: Output Parameters v_s and α, Which Are Defined in the Text, of the Fitted TOF Distribution of the Incident Beam[a]

mixture composition	v_s/ms^{-1}	α/ms^{-1}	h	$T_{parallel}$/K	$\langle E_i \rangle$/ kJ mol^{-1}
7% NO, 28% He, 65% H_2	1754 (1748)	106	16.5	20	47 (46)

[a] The physical quantities, which are calculated from the output parameters, characterizing the incident beam are, the hydrodynamic speed ratio, h, the parallel temperature, $T_{parallel}$, and the mean kinetic energy, $\langle E_i \rangle$. The values in parentheses for the central velocity, v_s, and mean kinetic energy, $\langle E_i \rangle$, are the theoretical values as predicted by eq 6.

inelasticity factor, γ. The inelasticity factor gives the extent of the inelastic process between the two extreme cases: pure elastic scattering with $\gamma = 1$ and $\alpha_1 \approx 0$, and highly inelastic scattering as in the case of trapping desorption, with $\gamma = 0$ and $\alpha_1 = (2k_B T_s/m)^{1/2}$. Therefore, in the case of trapping desorption, the response function would depend only upon the final velocity (i.e., the molecule loses the memory of its initial conditions). Indirect inelastic scattering is an intermediate case with $0 < \gamma < 1$.

In the case of pure trapping desorption, the first term of eq 6 would be of the same form as the second term, which is in fact used to describe purely Maxwellian scattering for which equilibration of the molecule with the surface occurs. The second term of eq 6 contains the Maxwellian intensity factor, A_2, and the Maxwellian width, α_2, which is of the same form as α_1. It is evident that α_2 and α_1 are different in the presence of bimodal scattering (direct inelastic scattering and trapping desorption occurring at the same time). In the case of pure trapping desorption mechanisms, the two terms of the response function will be identical.

The detected scattered signal, $N(t)$, is the convolution of the response function with the velocity distribution, $D(t_0)$, of the incident beam at the surface. This term is called the dosing function and has the same form as that used for the incident beam. $N(t)$ can then be written as

$$N(t_f) - \int_0^{t_f} D(t_0)\, R(v_i(t), v_f(t))\, \frac{dt}{t - t_0} \tag{7}$$

where t_0 is the arrival time of the gas pulse at the surface and $D(t_0)$ is simply the convolution of the hat function due to the chopper where the gas pulse is generated and the velocity distribution of the incident beam at the surface. This allows the fitting of the TOF acquired data. The output parameters are then employed to generate a model of the scattered velocity distributions, $R(v_i, v_f)$, which are used to calculate the mean final velocity, $\langle v_f \rangle$, and the mean square final velocity, $\langle v_f^2 \rangle$ as defined by

$$\langle v_f \rangle = \frac{\int_0^\infty v_f R(v_f)\, dv_f}{\int_0^\infty R(v_f)\, dv_f} \tag{8}$$

and

$$\langle v_f^2 \rangle = \frac{\int_0^\infty v_f^2 R(v_f)\, dv_f}{\int_0^\infty R(v_f)\, dv_f} \tag{9}$$

From eq 9, the mean final translational energy, $\langle E_f \rangle$, can be determined.

Measurements of TOF of the scattered NO were made for a variety of incident translational energies up to that reported in Figure 1a and Table 1. However, only with this 47 kJ mol^{-1} incident beam, it was possible to record TOF data. Figure 1b shows the TOF profile of NO scattered from the Rh(111)−CCH_3 surface at 300 K at this incident energy. Although the figure does not illustrate it, we must emphasize that, in comparison with the previous measurements on the Pt-based systems,[25,26] the scattering intensity from the Rh(111)−CCH_3 surface has decreased by a factor in excess of 10-fold given near identical molecular beam and laser pulse intensities. For comparison, Figure 1c shows the TOF profile of NO scattered from a Pt(111)−CCH_3 surface at 300 K [25] for the same incident beam energy of 47 kJ mol^{-1}. Unfortunately, it is difficult to compare these data sets directly as steps had been taken to reduce the gas pulse width, from 56 to 28 μs, and to reduce the flight path, from 365 to 340 mm, between the measurements reported in parts c and b of Figure 1. However, given the preceding information, it is very likely that the two TOF profiles represent scattering by the same mechanism. To test this idea, a reconvolution analysis is required. Figure 2 shows the modeling of the scattered NO from Rh(111)−CCH_3 in the case of pure direct inelastic scattering assuming the same inelasticity as for the CCH_3 adlayer on the Pt(111) surface reported in our previous work[25,26] (Figure 2a) and in the case of pure trapping desorption scattering from a 300 K surface (Figure 2b). The reconvolution analysis utilized the incident beam conditions in Figure 1a and Table 1. It is quite clear from the comparison in Figure 2 that the NO scattering from the Rh(111)−CCH_3 surface occurs largely via

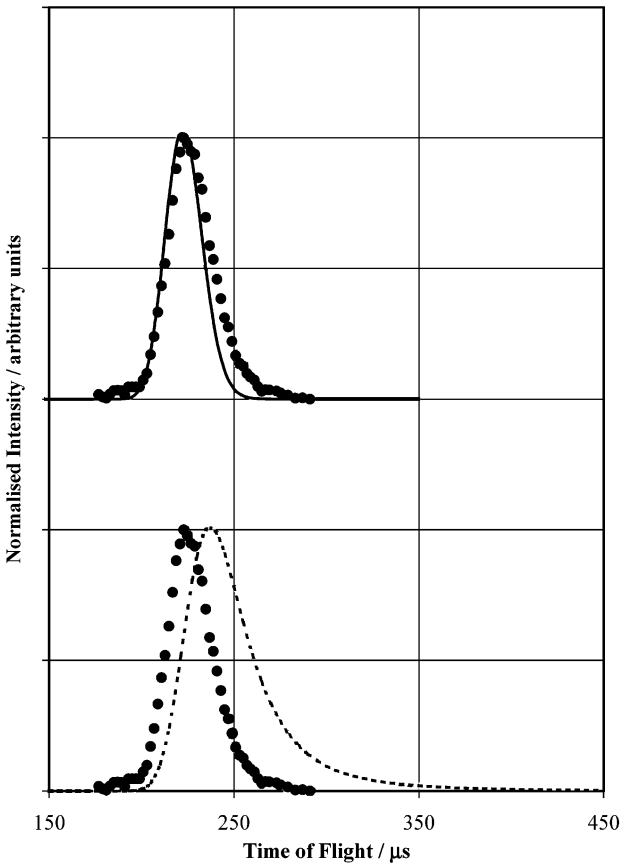

Figure 2. Modeling of the scattered NO TOF profile from Rh(111)−CCH_3. The solid line and dashed line are the direct inelastic scattering and trapping desorption models, respectively. Solid circles are the experimental data from scattering of the 7% NO in He and H_2 molecular beam used in Figure 1.

a direct inelastic channel. The slight broadening at long times may hint at a component of trapping desorption scattering with a thermal velocity characteristic of the surface temperature. Indeed, Figure 3 would appear to confirm this as a slight narrowing of the distribution of the high-J'' TOF profile (open circles) appears to be consistent with the loss of the residual trapping desorption channel component.

Why should we observe, as already mentioned, a reduction in scattering intensity by a factor in excess of 10 compared with the scattering on a Pt-based system, given similar molecular beam and laser intensities? Our previous studies of NO on CO and CCH_3 chemisorbed on Pt(111)[25,26] had shown that, as the incident translational energy was reduced at constant surface temperature, trapping desorption scattering became more important especially when the translational energy was comparable to or less than the interaction well depth. Indeed, at low surface temperatures and at incident energies on the order of the well depth, trapping desorption was the only observed scattering mechanism. We see no reason this should not be the case in the present work. The efficacy with which we could observe trapping desorption, in parallel with direct inelastic scattering, in our previous experiments was associated with the short (submicrosecond) residence time for the NO on the adlayer surface. This was entirely consistent with the small interaction well depths we predicted from this previous work. In the present study, as we observe a much-reduced scattering intensity into the direct inelastic channel and at low incident translational energies almost no scattering at all, it seems reasonable to conclude that trapping desorption, with a NO residence time (hundreds of microseconds or even milliseconds) much in excess

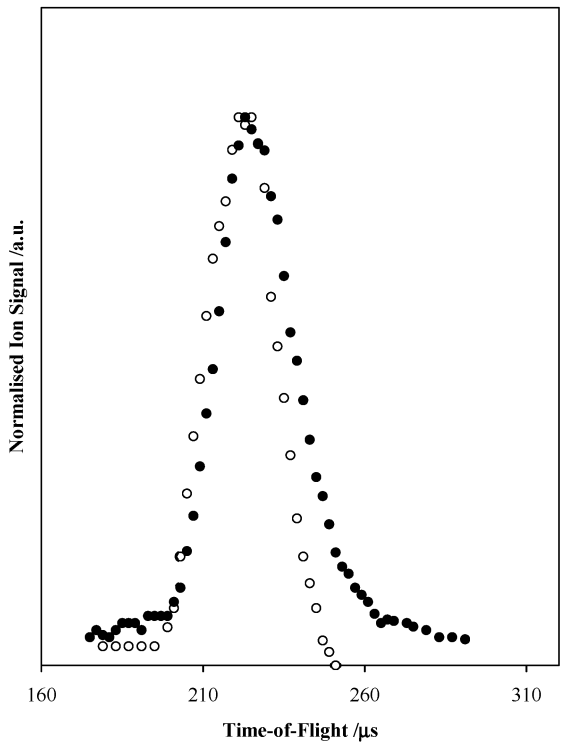

Figure 3. Comparison between TOF profiles of NO scattering into high-J'' (open circles) and low-J'' (filled circles) rotational states at 300 K.

of the time scale of our experiment, dominates the interaction with the Rh(111)−CCH_3 adlayer surface.

Later in this paper, we show using TPD that the potential well depth for NO on the Rh-based systems is at least 4 times greater than that of the Pt-based system at ca. 36 kJ mol^{-1}, independent of the adlayer system on Rh(111). Similar TPD measurements on the Pt(111) systems had previously proven impossible on our apparatus, confirming that at least qualitatively the interaction of NO with the adlayers on Rh(111) was much stronger than with the same adlayers on Pt(111). Therefore, we can conclude that the residence time of the NO on the Rh surface is much longer than for the Pt-based systems. As a consequence, the rate of desorption, k_{des}, is much smaller. For the Pt-based systems, we assumed that trapping desorption occurred with residence time of less than a few microseconds (i.e., $k_{des} > 10^6\ s^{-1}$). A simple numerical study of the effect of the residence time on trapping desorption scattering from a 300 K surface, shown in Figure 4, suggests that even a relatively modest decrease in k_{des} to $10^4\ s^{-1}$ will broaden and flatten the TOF distribution. Such a broad TOF distribution will be difficult to distinguish against the noisy background of our experiments.

In the case of NO scattering from the Rh(111)−CO adlayer, there is no evidence of any appreciable scattered signal for any incident translational energy at a surface temperature of 300 K. This is consistent with an extreme broadening of the TOF profile due to the residence time effects.

As discussed later in this paper, the observation of similar well depths for NO adsorption on the CO and CCH_3 adlayers from TPD measurements does not invalidate this conclusion as changes in the preexponential factor could easily account for the observation.

One logical step to consider would have been to conduct our scattering measurements from higher temperature surfaces or to increase the incident translational energy of the NO. However, given the nature of the adlayer−Rh surface, increasing the

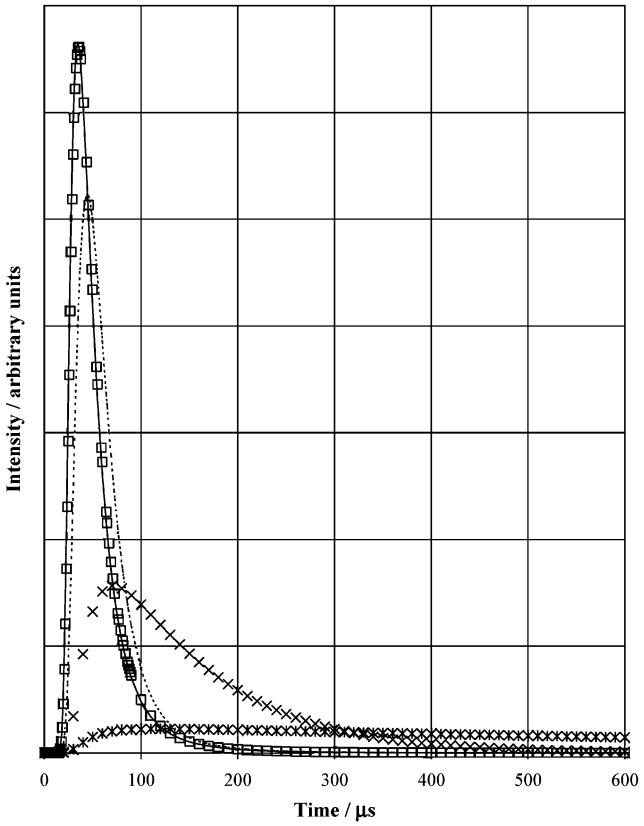

Figure 4. Numerical modeling of the effect of the surface residence time on the time-of-flight distribution resulting from the scattering of an incident beam characterized by Figure 1a and Table 1, in a trapping desorption channel from a surface at 300 K. The solid line is for a desorption rate, k_{des}, of 10^7 s^{-1}, the open squares for a k_{des} of 10^6 s^{-1}, the dotted line for a k_{des} of 10^5 s^{-1}, the times signs for a k_{des} of 10^4 s^{-1}, and the asterisks for a k_{des} of 10^3 s^{-1}.

surface temperature would lead to a change of the structure and/or composition of the adlayer itself. In the case of the CCH_3 adlayer, it has been shown that a surface temperature of 350 K is sufficient to decompose the ethylidyne species to produce C_2H and CH species.[34] In the case of the CO adlayer, RAIRS measurements performed in our laboratory have revealed that the structure of the adlayer is extremely sensitive to the surface temperature in the range of 300−400 K in terms of peak intensity and vibrational frequency. This has also been confirmed recently by Klotzer and co-workers,[35] where, for a saturated CO adlayer, temperature-programmed desorption experiments have shown a substantial CO desorption in the temperature range of 300−350 K and a peak temperature of 380 K. To increase the translational energy of the incident NO would have required us to heat our nozzle, which would inevitably have resulted in undesirable population of high-J'' rotational energy states and hence broadening of the incident rotational energy distribution.

Given the difficulties encountered in obtaining TOF data, it was only possible to carry out the rotational state distribution analysis for the 47 kJ mol^{-1} NO beam scattering from the Rh(111)−CCH_3 surface at 300 K. The procedure and reliability in extracting the rotational quantum state populations of the incident and scattered NO molecules via laser detection have been described elsewhere.[26] The resulting values of the rotational population, $n_{J''}$, are presented in Boltzmann format by plotting values of $\log[n_{J''}/(2J''+1)]$ as a function of the rotational energy, E_{rot}. In the case of a system exhibiting Boltzmann behavior (i.e., a straight-line plot), this allows assignment of a rotational temperature, T_{rot}, to the quantum state distribution of the molecule. The distributions are also characterized in terms of average rotational energies, defined as

$$\langle E_{rot}\rangle = \frac{\sum_{\Omega}\sum_{J''} n_{J''} E_{rot}(J'')}{\sum_{\Omega}\sum_{J''} n_{J''}} \qquad (10)$$

where $E_{rot}(J'')$ is the rotational energy of the NO molecule in the J'' state of a particular spin−orbit (Ω) state. The summations are over all the rotational and spin−orbit states. Of course, for a Boltzmann distribution, this average is characterized by the rotational temperature. For a non-Boltzmann distribution, temperature has no meaning and the average rotational energy is the better descriptive quantity.

Figure 5 shows the REMPI spectrum of NO scattered from Rh(111)−CCH_3 with an incident translational energy of 47 kJ mol^{-1} at a surface temperature of 300 K. Although the signal-to-noise ratio is poor, it does not preclude further analysis of the spectrum, and the rotational state distribution derived from Figure 5 is shown as a Boltzmann plot in Figure 6b. The rotational temperature obtained from this Boltzmann plot is 340 ± 20 K, and the average rotational energy, $\langle E_{rot}\rangle$, calculated by means of eq 10, takes a value of 200 cm^{-1} (= 2.4 kJ mol^{-1} ≈ k_BT as would be expected for a Boltzmann distribution of rotational energy levels). For comparison, Figure 6a displays the rotational state distribution derived from the scattering of a 50 kJ mol^{-1} NO beam incident on a Pt(111)−CCH_3 surface at 300 K as reported in our previous work.[26] The rotational temperature and the rotational energy values are in this case 610 K and 4.7 kJ mol^{-1}, respectively. This latter result has been previously explained in terms of scattering exclusively by a direct inelastic mechanism[25,26] in which the incident translational energy of the NO molecule is efficiently converted into rotational energy as a consequence of angular anisotropy in the repulsive part of the gas−surface potential. In the case of NO scattering from Rh(111)−CCH_3 at 300 K, the rotational temperature and the average rotational energy derived from the analysis of the REMPI spectra of scattered NO with an incident energy of 47 kJ mol^{-1} indicate that scattering may well be occurring via a trapping desorption mechanism in which multiple collisions with the surface, or indeed a substantial residence time on the surface, results in equilibration of the scattered molecules with the surface. In the case of Pt(111)−CCH_3, trapping desorption appears to be important only if the incident translational energy is limited to 10 kJ mol^{-1} for scattering at 300 K. Both qualitatively on the basis of scattering experiments[32] and quantitatively on the basis of the simple hard cube model,[25,32] the NO binding energy on the CCH_3 overlayer on Pt(111) is estimated to be around 10 kJ mol^{-1}, and so of a magnitude similar to that of the NO binding energy in the NO/Ag(111) system. It is therefore reasonable to assume that, given the predominance of the trapping desorption channel in the case of NO scattering from the CCH_3 overlayer on Rh(111) under the conditions reported herein, the interaction of NO with this substrate is considerably stronger at 30−50 kJ mol^{-1}.

II. Static Interaction of NO with CCH_3 and CO Overlayers on Rh(111). In the previous section we demonstrated that NO undergoes trapping desorption from both the Rh(111)−CCH_3 and Rh(111)−CO adlayer systems, and we presented evidence of long (hundreds of microseconds or milliseconds or longer) residence times on those surfaces. It is therefore reasonable to suppose that, at low surface temperatures (ca. 100 K), the molecule may reside on the surface for a time scale that is sufficiently long enough to observe it with static techniques. In this section we present such measurements of

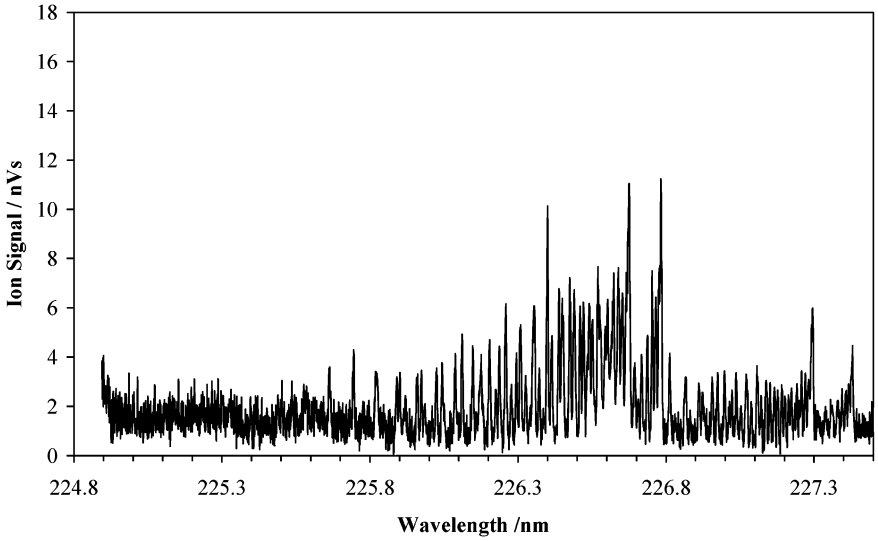

Figure 5. REMPI spectrum of NO scattering from Rh(111)−CCH_3 with an incident energy of 50 kJ mol^{-1}.

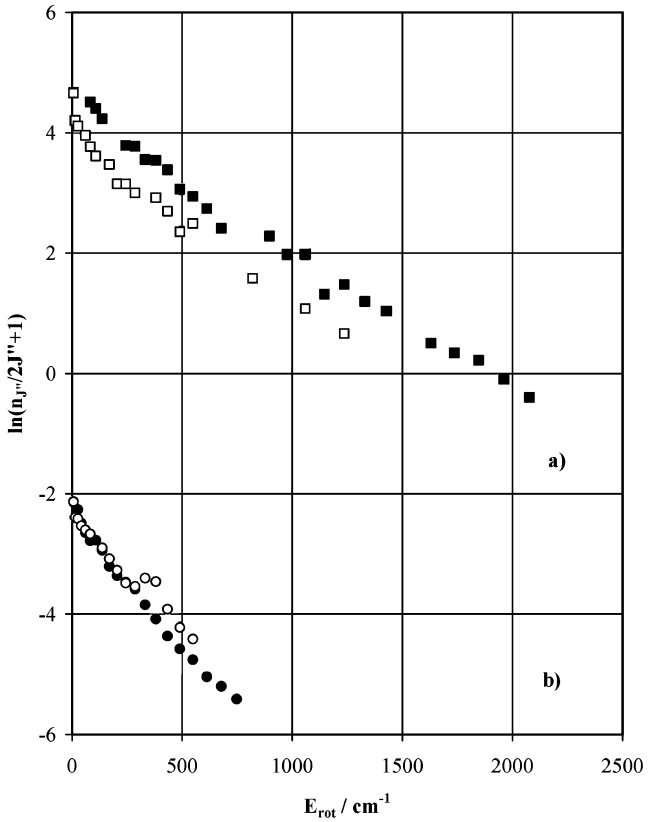

Figure 6. Boltzmann plots of the rotational state distributions of NO scattering from (a) Pt(111)−CCH_3 at 300 K with an incident energy of 50 kJ mol^{-1}, taken from ref 26, and (b) Rh(111)−CCH_3 at 300 K with an incident energy of 50 kJ mol^{-1}. The filled circles and squares correspond to J'' states from the $^2\Pi_{1/2}$ spin−orbit state, while the open circles and squares correspond to those from the $^2\Pi_{3/2}$ state.

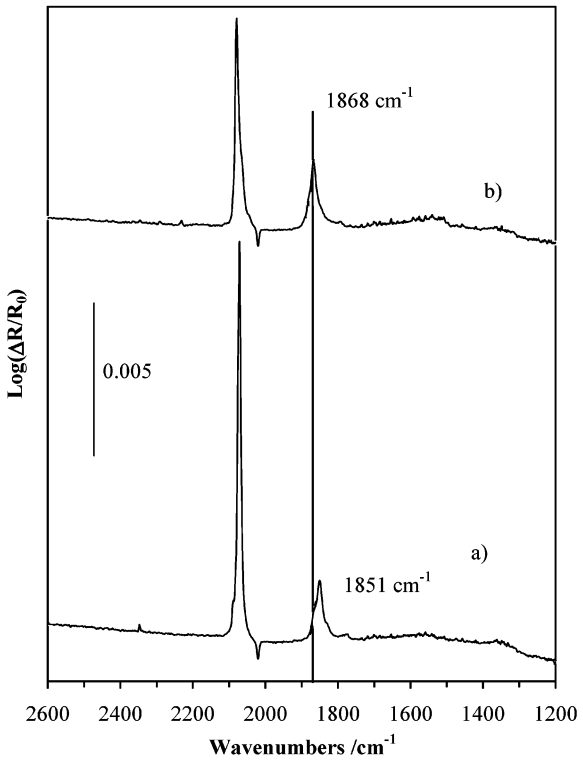

Figure 7. RAIR spectra recorded at 120 K of (a) 10 langmuirs of CO on Rh(111) adsorbed at 300 K and (b) 30 langmuirs of NO on Rh(111)−CO adsorbed at 120 K.

the static interaction of NO on CCH_3 and CO adlayers on Rh(111) at 120 K by means of RAIRS, TPD, and CID.

The adsorption of NO on Rh(111)−CCH_3 at 120 K as studied using RAIR and Auger spectroscopies has been reported in a previous paper.[36] Therein, it was concluded that the NO molecule adsorbs as a second surface adlayer on top of the ethylidyne with its internuclear axis lying parallel to the surface. The main observation was that this particular adsorption state gives rise to the asymmetric C−H stretch of the methyl group, which is forbidden in RAIR spectroscopy by the metal surface selection rule. In addition, no vibrational feature associated with the NO molecule could be found in the RAIR spectra, even if the surface was held at equilibrium with a pressure of 1×10^{-6} Torr of NO. Auger spectroscopy was then used to reveal the NO molecule adsorbed onto the CCH_3 adlayer at 120 K, and by comparing the NO peak intensities with and without the ethylidyne adlayer, a coverage estimate of NO in this second adlayer adsorption state was found to be 0.3 ML.

Figure 7a is the RAIR spectrum recorded at 120 K following a 10 langmuir exposure of CO on clean Rh(111) at room temperature. This spectrum exhibits two characteristic bands: the C−O stretches of the molecule adsorbed on the atop site at 2070 cm^{-1} and on the 3-fold site at 1850 cm^{-1}, in agreement with recent HREELS data.[37] Figure 7b is the RAIR

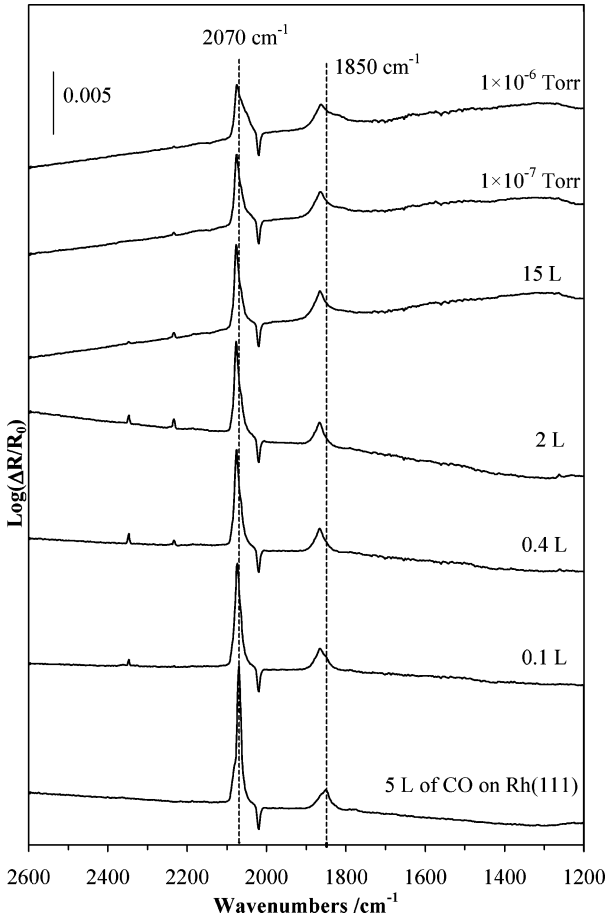

Figure 8. RAIR spectra recorded at 120 K of NO adsorption at 120 K on Rh(111)−CO at different NO exposures as indicated in the margin. The bottom spectrum is the CO adlayer formed at 300 K.

spectrum recorded at 120 K following a 30 langmuir exposure of NO on this Rh(111)−CO adlayer. Comparing the two spectra, a substantial decrease in the intensity of the band associated with the molecule bound on an atop site is evident. The intensity is less than half the intensity prior to exposure of the surface to NO. Conversely, the resonance relative to the 3-fold site adsorption is unchanged in terms of intensity but is shifted to higher frequency by about 20 cm^{-1}. As in the case of the NO adsorption on Rh(111)−CCH_3 at 120 K, there appears to be no resonance which can be identified with the NO molecule.

This postdosing experiment was repeated under the same conditions, increasing the number of steps at which the surface was dosed with NO at 120 K, up to dynamic NO pressures of 1×10^{-7} and 1×10^{-6} Torr. These results are shown in Figure 8. Again it can be clearly seen that, as the NO exposure is increased, the magnitude of the main CO band diminishes progressively, losing approximately 60% of its intensity with exposure to a dynamic pressure of 1×10^{-6} Torr of NO. It is also noticeable that this band becomes broader. The peak associated with the CO molecule bound in a 3-fold site does not change intensity but becomes slightly broader following the increase of the NO exposure. Surprisingly, despite the fact that the NO seems to have a considerable influence on the CO adlayer, there is no trace of any typical NO resonance even if the surface is exposed to a high dynamic NO pressure. Therefore, as in the case of the ethylidyne adlayer,[36] it is reasonable to suppose the NO molecules might bond as a second adlayer on top of the CO adlayer. If indeed the NO is sitting on the CO adlayer at 120 K, then it should be revealed, for example, by heating the surface. This experiment is shown in Figure 9.

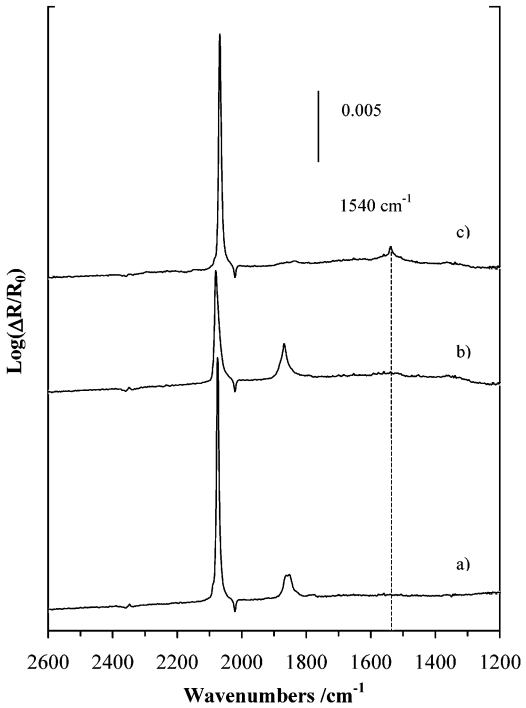

Figure 9. RAIR spectra recorded at 120 K of (a) 10 langmuirs of CO on Rh(111) adsorbed at 300 K, (b) 30 langmuirs of NO on Rh(111)−CO adsorbed 120 K, and (c) the same surface as in (b) after it was heated to 330 K.

The spectrum in Figure 9a is relative to that of the CO adlayer formed at 300 K and recorded at 120 K. The spectrum in Figure 9b follows a 30 langmuir exposure of NO on Rh(111)−CO at 120 K. Again a consistent decrease of the intensity of the main peak is observable. The spectrum in Figure 9c was recorded after the surface was heated at 330 K. From this spectrum the restoration of the main CO peak is clear; in addition, another small peak at 1540 cm^{-1} is visible. This feature can undoubtedly be assigned to the NO. The absence of the CO peak due to the CO adsorbed in 3-fold sites in Figure 9c is unsurprising since the temperature of 330 K is the temperature at which the CO molecules adsorbed in this particular site start to desorb.

The progressive decrease of the main CO peak as the NO exposure is increased could in principle be explained in terms of the variation of the refractive index of the surface due to the presence of the NO molecule, thus resulting in a diminished IR signal. If this were the case, then the entire spectrum might well be equally affected. In particular we might expect to see similar attenuation of the band associated with the CO molecule bound in a 3-fold site. However, this does not seem to be the case (Figures 7−9). On the other hand, one could suppose that the interaction of the NO molecule on top of the CO adlayer is such that the CO molecule bound on the rhodium surface is tilted and therefore its normal component of the dipole is reduced. However, if this were the only mechanism, then to have such a decrease in the intensity of the main CO band the CO molecule would have to be tilted with an angle greater than 45° (assuming direct proportionality between the intensity of the dipole moment and the intensity of the infrared band). The detailed mechanism of this intensity reduction therefore remains open to interpretation.

The appearance of the peak at 1540 cm^{-1} upon heating the surface can be simply explained by considering that the CO adlayer becomes more mobile and therefore the NO molecules, which sit in the second adlayer, now have opportunities to bind directly to the metal surface. Of course, it must be recognized

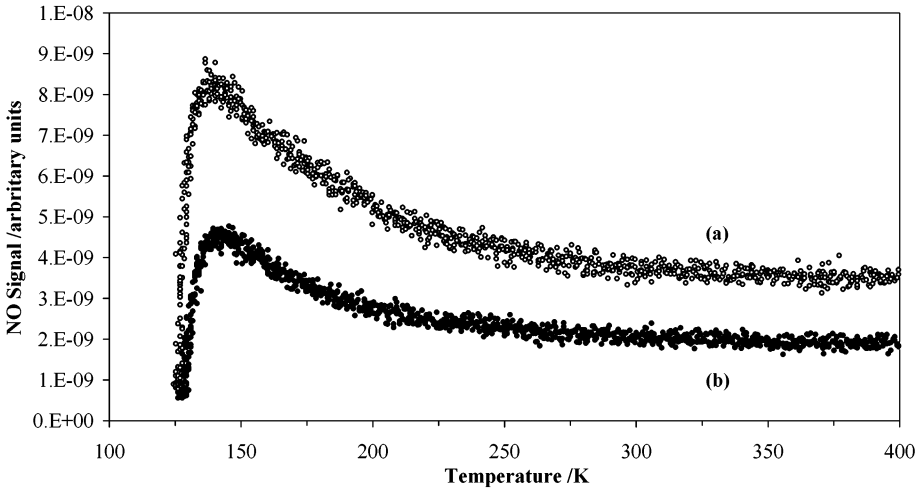

Figure 10. TPD profiles of NO desorbing from (a) Rh(111)−CO and (b) Rh(111)−CCH_3 surface adlayers.

that the majority of the NO molecules desorb as the surface temperature is raised and a very small portion of NO molecules can bind among the CO molecules in a thermally activated process. The frequency of this resonance is very close to that of the resonance of the NO adsorbed on clean Rh(111) at low surface temperature and low exposure,[38] and therefore, this assignment of the weak 1540 cm^{-1} feature does not seem unreasonable.

As in the case of the low surface temperature adsorption of NO on the CCH_3 adlayer, the observations in the case of the CO adlayer can only be explained by inferring that the NO molecule lies on top of the CO adlayer with its internuclear axis parallel to the surface. In this configuration, NO is perturbing the CO adlayer as a consequence of an induced dipolar interaction of the molecule adsorbed as a second adlayer. This induced dipolar interaction might be the result of some sort of rearrangement of the CO molecule due to the attraction between the NO and the Rh surface. It is not unreasonable to assume, however, that there remains a strong interaction between the NO molecule and the Rh metal surface.

At this point it is natural to consider the strength of the interaction between the NO and the CCH_3 and CO adlayers adsorbed on Rh. TPD profiles were recorded at 120 K, and detection of mass 30 was made in the line of sight. Prior to the TPD run and after dosing with NO, the sample was flashed at 135 K to minimize desorption from the heating wires and sample support. Figure 10 shows TPD traces from **(**a) the CO adlayer and (b**)** the CCH_3 adlayer. The two experiments were undertaken under the same experimental conditions in terms of surface preparation (same amount of NO dosed), detection (same mass spectrometer sensitivity), and NO background pressure just before the acquisition. The difference in intensity of the NO signal from the Rh(111)−CO is clearly evident and is reproducible. It should be stressed that there is no offset in the data of Figure 10. Therefore, this observation suggests the amount of NO desorbing from the CO adlayer is greater than that from the CCH_3 adlayer. This in turn might explain the difference in the scattering dynamics of NO from those adlayers. If a greater fraction of NO molecules can adsorb on top of the CO adlayer, then a larger amount of NO molecules can be accommodated during trapping desorption scattering. The temperature of the desorption peak is approximately the same for the two TPD traces (144 K). The shape of the peaks suggests a first-order desorption process. Using a Redhead analysis,[39] a desorption energy of 36 kJ mol^{-1} is obtained assuming a preexponential factor of 10^{13} s^{-1} (with a heating rate of 4 K s^{-1}). However, the scattering experiments suggest that the residence time on the CO adlayer is longer than on the CCH_3 adlayer. This would point to differences in the preexponential factor for desorption. In particular, a larger preexponential factor for the CCH_3 surface (i.e., shorter residence time) could be associated with a larger change in entropy in forming the transition state for desorption. This might be easily explained if, in the adsorbed state, the torsional motion of the ethylidyne group is restricted by the adsorbed NO, but becomes more free as the NO moves into the transition state. The additional degree of freedom, which is not present in the CO adlayer, would increase the entropy of activation in the CCH_3 system over that of the CO. No such TPD could be made on the Pt-based systems as the binding energies are too small. However, well depths of the interaction potentials on the Pt-based systems have been estimated on the basis of a simple hard cube model[25] using the so-called differential accommodation law developed by Tully and coworkers.[40] Results have indicated a well depth of 7.2 kJ mol^{-1} for the CO adlayer and 6.7 kJ mol^{-1} for the CCH_3 adlayer.[25]

The CID technique was applied to investigate the binding energy of the adsorbed NO on Rh(111)−CCH_3 at 120 K. Experimentally, a molecular beam mixture of 3% Kr in H_2 with an incident energy of 370 kJ mol^{-1} was used to induce desorption of NO from Rh(111)−CCH_3 at 120 K. Two impact angles were chosen: the direction normal to the surface and 45° off the surface normal. Surprisingly, no signals due to NO molecules were observed in either experiment. Subsequently, a TPD experiment was run, and it revealed that the NO molecule was still present on the surface, with little change to the TPD profile previously recorded. Clearly, the collision process for desorption of NO from a second adlayer turns out to be particularly inefficient. The theory behind CID is based on classical concepts of binary collision events (hard sphere collisions). In this model, it is assumed that a desorption event involves two collisions. The first occurs between the projectile atom and the adsorbate and the second between the adsorbate species and the surface atom, which may eject the adsorbate into the gas phase.[41−43] In the case of the present study, it appears realistic that the second collision between the NO molecule and the ethylidyne adlayer does not transfer enough energy to the NO molecule for it to escape the surface. Therefore, this process can be thought of as occurring in a very soft adlayer surface (the ethylidyne overlayer) where the energy of the first collision is easily dispersed, in comparison with collision-induced desorption of species from a "hard" metal surface.

Conclusions

The dynamics of the scattering of NO in a supersonic molecular beam from CCH_3 and CO chemisorbed on Rh(111) have been investigated at a surface temperature of 300 K using REMPI. Time-of-flight and rotational state distributions of NO molecules scattered at room temperature have been measured for incident energies up to 47 kJ mol^{-1}. Both sets of measurements have shown that the dynamics are strongly determined by the trapping desorption process, despite the relatively high incident energy and surface temperature. This behavior is distinctly different in comparison with the dynamics of NO from the same adlayers adsorbed on a Pt(111) surface previously reported.[25,26]

Reflection−absorption infrared spectroscopy investigations of the static interaction between NO and CO adsorbed on Rh(111) have revealed that NO adsorption takes place on the CO adlayer at 120 K. A similar behavior of NO on the CCH_3 adlayer chemisorbed on Rh(111) was reported in a previous paper.[36] The NO itself cannot be directly detected by RAIRS; rather its presence is manifest through the perturbation of the CO RAIR spectrum, suggesting that the NO molecules are lying on top of the adlayer with the internuclear axis parallel to the surface. The observation of an unusual second-layer state of NO on both substrates at low surface temperature indicates a strong interaction between the adlayer and the NO. Temperature-programmed desorption experiments have been used to estimate the NO activation energy for desorption from the adlayers. A value of 36 kJ mol^{-1} was found for desorption from both adlayers. However, TPD profiles have showed a substantial difference in the amount of NO desorbing from CO compared to CCH_3. The greater number of NO molecules desorbing from the CO adlayer is interpreted in terms of a greater propensity of the CO adlayer to accommodate the NO molecule. A longer accommodation time on the CO adlayer implies a smaller preexponential factor for desorption compared with desorption from the CCH_3 adlayer. This is interpreted assuming a greater change in entropy for desorption from the ethylidyne adlayer. Finally, collision-induced desorption experiments have not revealed any appreciable NO signal due to desorption from the Rh(111)−CCH_3 surface, despite the high incident translational energy of the krypton atoms. This suggests a very "soft" ethylidyne adlayer in which collisions with NO result in insufficient energy transfer to the NO molecule to permit desorption.

Acknowledgment. We thank the U.K. Engineering and Physical Sciences Research Council for equipment grants, and V.F. thanks the University of Nottingham for a research scholarship.

References and Notes

(1) Zare, R. N.; Dagdigian, P. J. *J. Chem. Phys.* **1974**, *185*, 739.
(2) Auerbach, D. Velocity Measurements by Time-of-flight Methods. In *Atomic and Molecular Beam Methods*; Scoles, G., Ed.; Oxford University Press: Oxford, U.K., 1988; Vol. 1, Chapter 14.
(3) *Dynamics of Gas−Surface Interaction*; Rettner C. T., Ashfold, M. N. R., Eds.; The Royal Society of Chemistry: Cambridge, U.K., 1991.
(4) Hurst, J. E.; Becker, C. A.; Cowin, J. P.; Janda, K. C.; Warthon, L.; Auerbach, D. J. *Phys. Rev. Lett.* **1979**, *43*, 1175.
(5) Barker, J. A.; Auerbach, D. J. *Surf. Sci. Rep.* **1985**, *4*, 1.
(6) Spruit, M. E. M.; Kuipers, E. W.; Tenner, M. G.; Kimman, J.; Kleyn, A. W. *J. Vac. Sci. Technol.* **1987**, *A5*, 496.
(7) Kimman, J.; Rettner, C. T.; Auerbach, D. J.; Barker, J. A.; Tully, J. C. *Phys. Rev. Lett.* **1986**, *57*, 2503.
(8) Rettner, C. T.; Kimman, J.; Fabre, F.; Auerbach, D. J.; Barker, J. A.; Tully, J. C. *J. Vac. Sci. Technol.* **1987**, *A5*, 508.
(9) Kleyn, A. W.; Luntz, C.; Auerbach, D. J. *Surf. Sci.* **1985**, *152*, 99.
(10) Rettner, C. T.; Fabre, F.; Kimman J.; Auerbach, D. J. *Phys. Rev. Lett.* **1985**, *55*, 1904.
(11) Spruit, M. E. M.; Kuipers, E. W.; Tenner, M. G.; Kleyn, A. W. *Surf. Sci.* **1988**, *205*, 241.
(12) Rettner, C. T.; Kimman, J.; Auerbach, D. J. *J. Chem. Phys.* **1991**, *94*, 734.
(13) Serri, J. A.; Cardillo, M. J.; Becker, G. E. *J. Chem. Phys.* **1981**, *77*, 1982.
(14) Asscher, M.; Guthrie, W. L.; Lin, T. H.; Somorjai, G. A. *J. Chem. Phys.* **1983**, *78*, 6992.
(15) Brenig, W.; Kasai, H.; Muller, H. *Surf. Sci.* **1985**, *161*, 608.
(16) Kuipers, E. W.; Tenner, M. G.; Kleyn, A. W. *Phys. Rev. Lett.* **1989**, *62*, 2152.
(17) Tenner, M. G.; Kuipers, E. W.; Kleyn, A. W.; Stolte, S. *J. Chem. Phys.* **1991**, *94*, 5197.
(18) Kleyn, A. W.; Luntz, C.; Auerbach, D. J. *Surf. Sci.* **1982**, *117*, 33.
(19) Frenkel, F.; Hager, J.; Krieger, W.; Walther, H.; Campbell, C. T.; Ertl, G.; Kuipers, E. W.; Senger, J. *Phys. Rev. Lett.* **1981**, *46*, 152.
(20) Senger, J.; Robota, H.; Vielhaber, W.; Ertl, G.; Frenkel, F.; Hager, J.; Krieger, W.; Walther, H. *Surf. Sci.* **1983**, *131*, 273.
(21) Butler, D. A.; Barenbak, B.; Stolte, S.; Kleyn, A. W. *Phys. Rev. Lett.* **1997**, *78*, 4653.
(22) Cohen, S.; Naaman, R.; Sagiv, J. *Phys. Rev. Lett.* **1987**, *58*, 1208.
(23) Cohen, S.; Naaman, R.; Sagiv, J. *J. Chem. Phys.* **1988**, *88*, 2757.
(24) Cohen, S.; Naaman, R.; Balint-Kurti, G. G. *J. Chem. Phys.* **1989**, *134*, 119.
(25) Ainsworth, M. K.; McCombie, J.; McCoustra, M. R. S.; Chesters, M. A. *J. Chem. Phys.* **2000**, *112*, 6031.
(26) Ainsworth, M. K.; McCombie, J.; McCoustra, M. R. S.; Chesters, M. A. *J. Chem. Phys.* **2000**, *113*, 8762.
(27) Oakes, D. J.; McCoustra, M. R. S.; Chesters, M. A. *Faraday Discuss.* **1993**, *96*, 325.
(28) Newell, H. E.; Oakes, D. J.; Rutten, F. J. M.; McCoustra, M. R. S.; Chesters, M. A. *Faraday Discuss.* **1996**, *105*, 193.
(29) Koestner, R. J.; Van Hove, M. A.; Somorjai, G. A. *Surf. Sci.* **1982**, *121*, 321.
(30) Kim, Y. J.; Thevuthasan, S.; Herman, G. S.;. Peden, C. H. F.; Chambers, S. A.; Belton, D. N.; Permana, H. *Surf. Sci.* **1996**, *359*, 269.
(31) *Atomic and Molecular Beam Method*; Scoles, G., Ed.; Oxford University Press: Oxford, U.K., 1988; Vol. 1.
(32) Ainsworth, M. K. Ph.D. Thesis, University of Nottingham, Nottingham, U.K., 1998.
(33) *Atomic and Molecular Beam Method*; Scoles, G., Ed.; Oxford University Press: Oxford, U.K., 1992; Vol. 2, Chapter 15, p 451 ff.
(34) Somorjai, G. A.; Van Hove, M. A.; Bent, B. E. *J. Phys. Chem.* **1988**, *92*, 973.
(35) Klotzer, B.; Unterberger, W.; Kayek, K. *Surf. Sci.* **2003**, *532*, 142.
(36) Fiorin, V.; McCoustra, M. R. S.; Chesters, M. A. *J. Phys. Chem. B* **2003**, *107*, 7058.
(37) Linke, R.; Curulla, D.; Hopstaken, M. J.; Niemantsverdriet, J. W. *J. Chem. Phys.* **2001**, *115*, 8209.
(38) Kim, Y. J.; Thevuthasan, S.; Herman, G. S.; Peden, C. H. F.; Chambers, S. A.; Belton, D. N.; Permana, H. *Surf. Sci.* **1996**, *359*, 269.
(39) Redhead, P. A. *Vacuum* **1962**, *12*, 203.
(40) Grimmelmann, E. K.; Tully, J. C.; Cardillo, M. J. *J. Chem. Phys.* **1980**, *72*, 1039.
(41) Beckerle, J. D.; Johnson, A. D.; Ceyer, S. T. *Phys. Rev. Lett.* **1989**, *62*, 685.
(42) Szulczewsky, G.; Levis, R. J. *J. Chem. Phys.* **1993**, *98*, 5974.
(43) Szulczewsky, G.; Levis, R. J. *J. Chem. Phys.* **1994**, *101*, 11070.